Arabian Journal for Science and Engineering
https://doi.org/10.1007/s13369-024-09507-3

RESEARCH ARTICLE-ELECTRICAL ENGINEERING

Detection and Classification of EHV Transmission Line Faults Based on Sign of Reactive Power

Rajesh Velpula[1,2] · **Nareddy Nageswara Reddy**[3] · **Raja Pitchaimuthu**[1,2]

Received: 28 October 2023 / Accepted: 6 August 2024

Abstract
In the outdoor erected overhead transmission lines, the probability of occurrence of a fault is high and it might lead to unstable operation of the power system and interrupt the continuity of power supply. This work has proposed a methodology to detect and classify such transmission line faults based on the signs of computed reactive power. The sign of reactive powers at both ends of the transmission line is computed through the extracted fundamental components of voltage and current obtained through the DFT algorithm. The discrimination of fault and normal operating conditions is achieved based on the signs of reactive power at both ends of the transmission line. Further, a transmission line fault classification strategy has been developed with the signs of computed reactive power. The method developed has been tested on the designed two-machine transmission test system and modified WSCC-9 bus test system in the PSCAD/EMTDC and MATLAB tools for all types of short circuit faults at various locations on the transmission line, with and without fault resistance, sudden change in load, with noisy input signal, CT saturation conditions, etc. In all the cases, the proposed method ensures the accuracy of detecting and classifying transmission line faults.

Keywords Fault detection · Fault classification · Transmission line protection · Reactive power · Fault resistance · PMU (phasor measurement unit)

1 Introduction

The transmission line (TL) is an essential element which connects the generation and the consumer point. Moreover, it is a geographically long element in power systems and spreads over hundreds of kilometers. When a fault occurs, the voltage (V) and current (I) signals deviate from their actual values, which can lead to an unstable condition or a blackout if the protection system cannot quickly isolate the faulty section. Therefore, the protection scheme developed by the protection engineer should retain the properties like accuracy, sensitivity, selectivity and reliability.

The TL protection scheme based on digital distance relaying consists of majorly three elements: fault detection, classification and localization. Out of the three elements, fault detection and classification mechanisms decide the speed and accuracy of the digital protective relaying scheme [1]. Therefore, quick removal of faulty phase becomes inevitable, enhance the quality of endowed power and boost the system's stability. Up to now, various researchers have proposed many methods to detect and categorize TL defects by utilizing the electrical components of the transmission system. The conventional protection schemes based on impedance [2], traveling waves [3] and distance [4] are widely used in transmission line protection. The methods proposed based on impedance and distance depend on system parameters. The accuracy of these methods is low during stressed conditions. The traveling wave-based methods required high sampling frequency to extract the features from the sensed signals. Due to this, the complexity and cost of the relay infrastructure may increase. Despite various approaches, consolidating

✉ Raja Pitchaimuthu
praja@nitt.edu

Rajesh Velpula
rajeshvelpula.nitt@gmail.com

Nareddy Nageswara Reddy
nageshreddy.nitt@gmail.com

1 Hybrid Electrical Systems Laboratory, Department of Electrical and Electronics Engineering, National Institute of Technology, Tiruchirappalli, Tamil Nadu 620015, India

2 National Institute of Technology, Tiruchirappalli, Tamil Nadu 620015, India

3 VNRVJIET, Hyderabad, Telangana 500090, India

Published online: 28 August 2024

all protection system functions into a single framework is still a challenge. Therefore, the proposed method takes into consideration of noise, HIF, various FIAs, CT saturation conditions, and proposed a parameter independent approach for recognizing and categorizing TL faults.

In the literature, the researchers used pre and post-fault data of V and I to activate the protection system since those wave-forms contain valuable information concerning the short circuit faults. Various methods available in the published reports to identify and categorize the TL faults are presented in [5, 6] and [7]. These methods are categorized into 3 and named prominent, hybrid and modern. Prominent methods used in literature are fuzzy logic, Wavelet and ANN to name a few. Hybrid methods consist of any two combinations of prominent methods, and the modern methods originated from Pattern recognition, Genetic Algorithm, SVM and PMU-driven protection approaches, etc. An overview on different techniques for fault identification, categorization and location are presented in [8]. The authors grouped most of the methods available in the literature into artificial intelligence (AI)-based techniques, signal processing based techniques and emerging computational intelligence methods.

The authors of [9, 10] used Wavelet Transform (WT) based methods for TL protection. The method in [9] considered 240 kHz as sampling frequency (f_s), which is very high for pragmatic implementation and the method operates based on a threshold value for fault detection. The method proposed in [10] involves a dedicated communication channel and high sampling frequency. High f_s increases the cost of infrastructure for practical applications. Traveling wave-based methods are presented in [11, 12]. The method proposed in [11] required a set value for fault detection. The methods in [11, 12] use high sampling frequency. Learning-based TL protection methods are presented in [13–18]. [13] presented a self-attenuation Convolution Neural Network (CNN) based feature extraction using DWT and training data. DWT is used to analyze the faulty data and it needs high f_s. The authors of [14] uses graph CNN and adopted V measurements for fault detection and unable to detect the HIF. Moreover, it needs training data for classification and localization of a fault. Authors of [15] have used the combination of WT decomposition and Chebyshev Neural network (ChNN) to detect and classify transmission line faults. Even though the methodology detects and accurately classifies faults, it needs a higher f_s for wavelet decomposition and huge data set is required for training as it uses ChNN. A deep learning-based intelligent methodology has been utilized in [16] to protect TLs using capsule network sparse filtering (CNSF). The method converted the half-cycle data into an image and estimated the system condition based on the image signature. The method proposed in [17] used principal component analysis (PCA) to categorize and locate the faults on TL, which requires large amounts of data to train the algorithm. In [18], the authors developed an unsupervised feature learning and convolution sparse auto-encoder based method for TL protection, which is system dependent. A methodology proposed in [19] uses machine learning and meta-heuristic algorithms to detect and classify faults and it uses voltage as a threshold value to detect faults. A long short-term memory (LSTM) artificial intelligence and deep learning-based method was proposed to detect and classify faults in [20] and it requires high data to train the algorithm. All learning-based methods need huge data which is system dependent to train the algorithm under different fault cases. Moreover, high data storage and handling capacity infrastructure may increase the cost of the overall protection scheme.

In [21], a differential relaying algorithm has been presented and it estimates the Discrete Teager Energy (DTE) with the help of the Hilbert-Huang transformation (HHT) approach to identify the fault. However, the method identifies the fault accurately and it requires a set value limit to differentiate fault and the normal condition of the system and it leads to a system dependent method. A multi-variable signal processing technique has been presented in [22] and used fault index derived with Stockwell, Hilbert transforms and alienation coefficients. The developed fault index has a threshold to detect the fault and has not addressed the HIF detection. A protection scheme based on a fault index derived from positive sequence admittance parameters is presented in [23]. The scheme considered the set limit to identify the fault and did not address the fault classification. A wide area backup protection scheme developed in [24] uses the ratio of injected fault component apparent power addition to the subtraction of the injected fault component apparent power of both ends of a line. A TL protection methodology developed in [25] used the single-end current measurements. A differential current-based protection scheme developed in [26] utilizes both ends current magnitude and phase angle data to identify the faults. In [27], the authors have been proposed an algorithm to detect and classify the TL faults by calculating phase mean indices (PMI) and used the global threshold setting for fault detection. A wide area backup protection method has been presented in [28] has utilized the change in V for fault area selection of the network. For faulty line section identification, the method used the least square technique to estimate the fault by using pre and post-fault line parameters data and the method has not addressed fault classification. In [29], a sequence current-based pilot relaying scheme has been presented using single-end current data. Still, it has a threshold set for sequence current signal ratios and can only discriminate symmetrical and unsymmetrical faults. A relaying algorithm proposed in [30] uses differential current ratio to discriminate between fault and normal situation and it requires a threshold. A set value centered

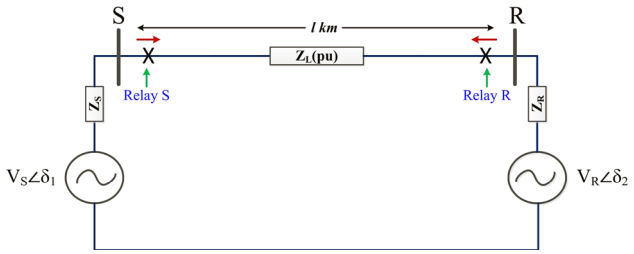

Fig. 1 A two-machine power system model

strategy to discriminate the symmetrical faults and overloads has been proposed in [31].

Majority of the TL detection and classification techniques developed by the researchers of protection group are training based such as deep learning, threshold set, dependent on-line parameters or having high sampling frequencies. Therefore, the proposed work attempts to make protection scheme which will work irrespective of f_s, independent of line parameters and able to detect the fault under different fault conditions like all types of shunt faults, faults with various fault inception angles (FIA), fault through high impedance, noisy input conditions, CT saturation and sudden change in load. The key benefits of the proposed method are listed below:

- Can be implemented without changing the existing protection infrastructure.
- Easily detects and classifies the transmission line faults under various operating conditions.
- Will not operate for the external faults.
- Works satisfactorily for HIFs, which is one of the problems in many existing methods.
- Able to work effectively with CT saturation and noise.
- Independent of system parameters.

Further the paper is organized with different sections. In Sect. 2, the motivation of the work and mathematical background of the proposed methodology are explained. Section 3 presents the methodology used for the proposed approach. Section 4 discussed the results to support the efficacy of the proposed methodology. The comparison of the proposed approach with various methods used in the previous works is provided in Sect. 5 and Sect. 6 concludes the highlights of the work.

2 Motivation and Mathematical Formulation

Here in this section a mathematical analysis has been attempted to realize the sign of reactive power at both ends of a TL during normal and faulted case. A two-machine doubly-fed transmission system model shown in Fig. 1 is considered for the analysis [32].

Let the terminal voltage of $V_S\angle\delta_1$ of source S, $V_R\angle\delta_2$ of source R, and the transmission line has an impedance of Z_L(pu).

$$\text{The apparent power supplied by the source} = VI^* \tag{1}$$

where V and I are voltage and current, respectively.

From Fig. 1, the amount of apparent power supplied by source S is

$$S_S = V_S\left[\frac{V_R - V_S}{jX}\right]^* = \frac{V_S V_R}{X}\sin\delta + j\left[\frac{V_S^2 - V_S V_R\cos\delta}{X}\right] \tag{2}$$

where $\delta = \delta_1 - \delta_2$

From the Eq. (2), the imaginary part represents the amount of reactive power supplied by source S, denoted by Q_S.

$$Q_S = \left[\frac{V_S^2 - V_S V_R\cos\delta}{X}\right] \tag{3}$$

Similarly, the apparent power supplied by the source R,

$$S_R = V_R\left[\frac{V_S - V_R}{jX}\right]^* = \frac{V_S V_R}{X}\sin\delta + j\left[\frac{V_R V_S\cos\delta - V_R^2}{X}\right] \tag{4}$$

The imaginary part of Eq. (4) represents the amount of reactive power supplied by source R, denoted by Q_R.

$$Q_R = \left[\frac{V_R V_S\cos\delta - V_R^2}{X}\right] \tag{5}$$

Equations (3) and (5) are the reactive powers derived and the following two cases has been considered to realize the reactive power sign.

Case i: During Normal Operation

Under normal operating conditions of the system, the voltage magnitude difference between both ends of a line is less. Moreover, during stable operation the systems load angle be between greater than zero and 90^0 [32], thus the value of $\cos\delta$ will be in between greater than zero and 1. Therefore, at normal operating conditions of the system, $V = V_R \approx V_S =$ 1 pu and the line reactance can be considered as constant. After substituting the assumed values in Eqs. (3) and (5), the signs of Q_S and Q_R are observed as positive and negative, respectively. Hence, it is concluded that the signs of reactive power supplied from the sources are positive and negative simultaneously during the normal operating conditions of the system. Besides, both sources meets the reactive power demand and line reactive power losses.

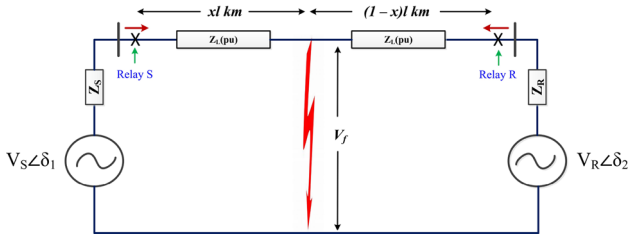

Fig. 2 Power system model representation during faulted situation

Case ii: During Fault Condition

Figure 2 shows the system during fault condition representing all system parameters, including the fault voltage denoted by V_f.

Let the value of the voltage at the fault point is V_f with respect to ground and $V_f \neq 0$ under non-bolted fault cases.

Now the reactive power supplied from the source S, i.e.,

$$Q_S = \left[\frac{V_S^2 - V_S V_f \cos\delta_1}{X}\right] \tag{6}$$

Similarly, the reactive power supplied from the source R,

$$Q_R = \left[\frac{V_R^2 - V_R V_f \cos\delta_2}{X}\right] \tag{7}$$

At the fault point, the value of fault voltage is either zero or significantly less, and it depends on the value of fault impedance, i.e., $V_S \approx V_R \gg V_f$.

From the above case study, during faulted conditions of the system, the reactive power supplied from both ends of the line or sources are positive. Moreover, the supplied reactive powers from both the ends will meet the reactive power losses of the line. During normal operating situations of the system, the reactive powers computed at both ends of the line are simultaneously positive and negative.

3 Proposed Methodology

The proposed method computes the reactive power sign based on the extracted fundamental components of V and I at both ends of the line from the synchronized PMU data. The synchronized fundamental components of measured signals are attained through a DFT algorithm. The method utilizes the fundamental components of V, I and phase angle data obtained from DFT to estimate the reactive powers of all the three-phases with sign at both the ends of the line using the expression shown in Eq. (8).

$$Q_{XY} = V_{XY} I_{XY} \sin\phi_{XY} \tag{8}$$

where X represents the Source 'S' or source 'R' and Y represents A or B or C phases.

The proposed method has three different steps to identify and classify the TL faults. First stage is the fault identification process, second is to discriminate the grounded or ungrounded fault and the third one is the fault classification process. For fault identification, the following strategy has been adopted to discriminate the normal and the faulted condition of the system. If the signs of Q at two ends of the line are positive then the method proposed identifies it as a fault, otherwise the method considers the system is in normal operation or external fault. Once the proposed method identifies the fault, it verifies if the fault is through ground, as per the summation of the instantaneous currents (SIC) measured at either ends of the line. The fault is treated as a grounded fault if SIC is zero, otherwise it is considered an ungrounded fault. Based on the decision from the second stage, the proposed method starts classifying the faults.

For the classification of the faults, the method follows the estimated sign of Q at two terminals of the line and the whole strategy of fault classification is shown in the flow chart given in Fig. 3. For instance, if the reactive powers of phase A at both the ends of the line alone are positive and the SIC is not equal to zero, then the method classifies the fault as AG. If the SIC is zero and the sign of Q at both the ends of the line for A and B phases are found to be positive and phase C is not positive then the method classifies the fault as AB fault. Similarly, the whole process of fault classification is followed as per the flow chart shown in Fig. 3.

4 Results and Discussions

4.1 Test System and Simulation Parameters

A two-bus test system of voltage 400 kV with a frequency of 50 Hz has been adopted to validate the proposed method. The PSCAD/EMTDC and MATLAB/Simulink softwares are used to simulate the adopted test system.

Figure 4 shows the two-bus test system considered, and the parameters used for the simulation are given in Table 1 [33]. A frequency-dependent TL model is adopted to enhance the accuracy of the simulation results [34]. Various simulation studies have been done under varied fault conditions, such as all conventional short circuit faults and CCFs at various locations of lines with distinct fault resistance (R_f)s and FIAs. A f_s of 1 kHz has been utilized for the entire simulation studies.

4.2 Validation of the Proposed Fault Detection Methodology

The proposed method has been verified with various fault cases, and the corresponding simulation results are presented in the subsequent sections.

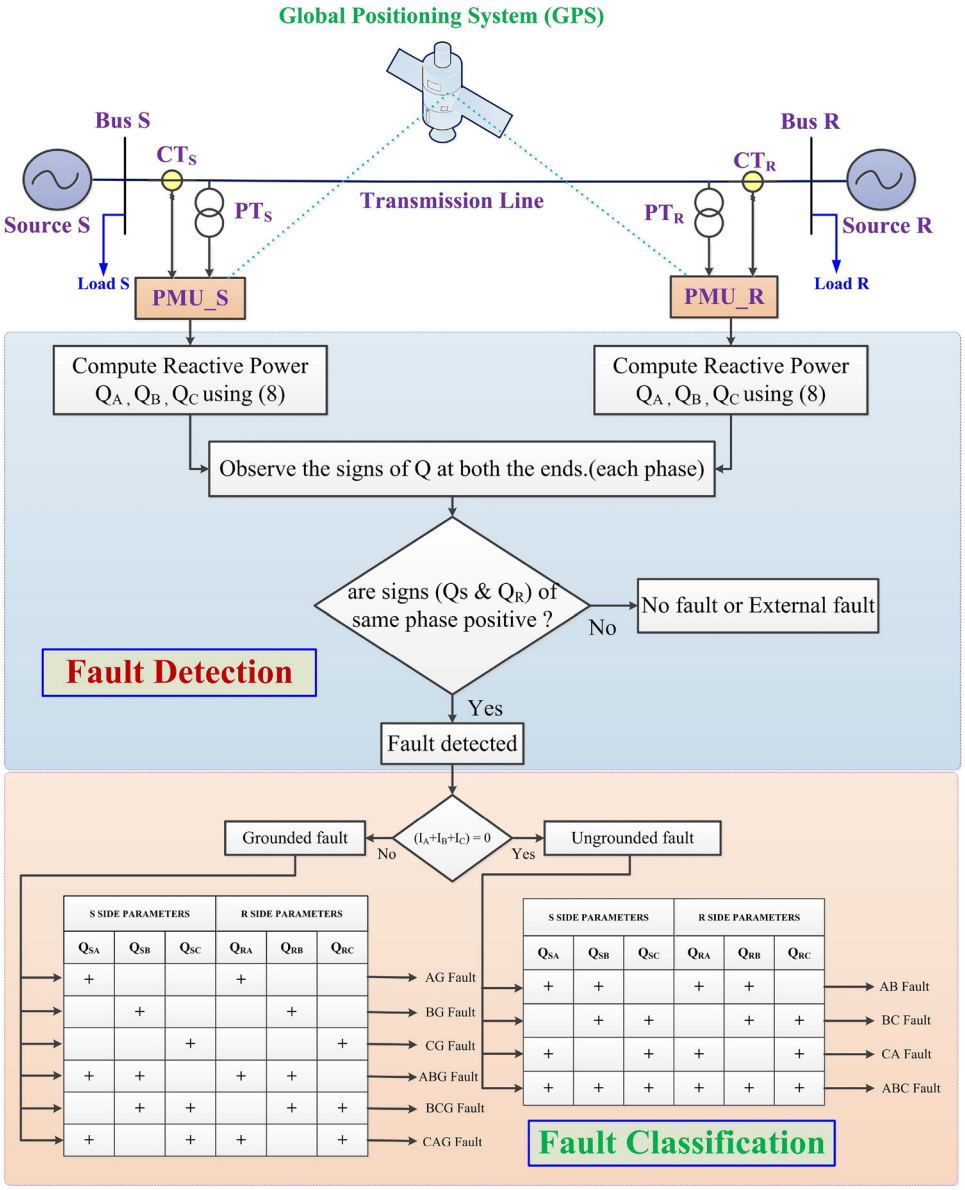

Fig. 3 Flowchart of proposed methodology

Case (i): Phase to Ground (PhG) Fault

The test power system designed has been simulated in PSCAD/EMTDC software environment. An AG bolted fault at 0.4s has been created at a distance of 0.5 pu on the TL from the bus S. The computed Q from the processed fundamental components at both ends of the TL are placed in Fig. 5.

Figure 5 shows that the computed Q of each phase from bus S is positive, and from bus R named Q_R is negative until the fault initiation, i.e., up to 0.4 s. After the fault inception, the sign of Q of phase A at both the buses is observed as positive, and the remaining two phases' Q flow remains the same. Based on the observations, the method detects this situation as a fault and gives the trip signal. Further, the proposed method is verified for an AG fault with 0.01 Ω, 10 Ω, 30 Ω, 50 Ω, 100 Ω and 200 Ω R_fs and the attained results are shown in Table 2.

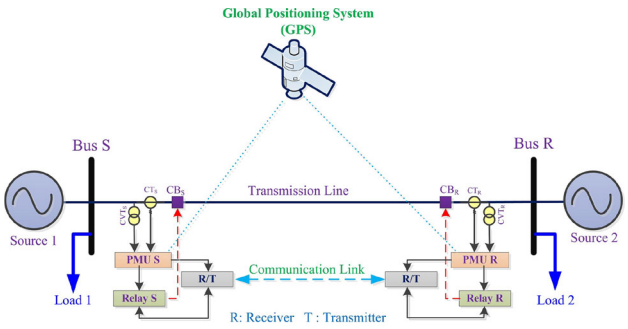

Fig. 4 Doubly fed two-bus test system

Table 1 Parameters of two-bus test system

Parameters	Value
Source parameters	
Source S terminal voltage	$400\angle 5^0$ kV
Source R terminal voltage	$400\angle 35^0$ kV
f (Hz)	50
Line and load parameters	
Length (km)	300
R_{l1} per km	0.03293 Ω
R_{l0} per km	0.2587 Ω
$X_{L_{l1}}$ per km	0.327 Ω
$X_{L_{l0}}$ per km	1.174 Ω
$X_{C_{l1}}$ per km	280.1 kΩ
$X_{C_{l0}}$ per km	461.254 kΩ
Per phase load at Bus S & R	100 MW, 25 MVAR

*Suffix l =line;1= positive sequence;0=zero sequence

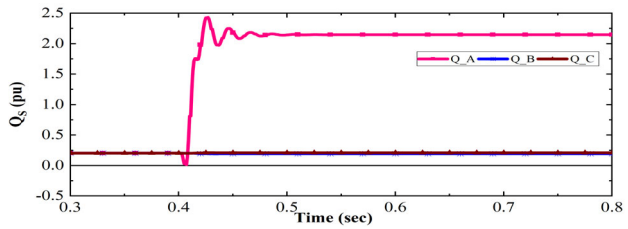

(a) Q_S

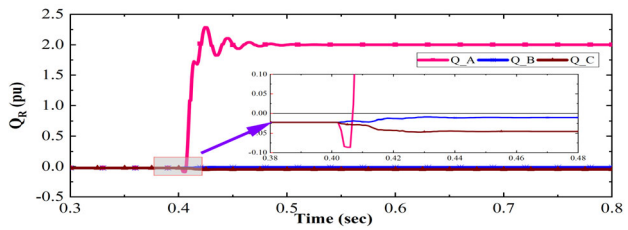

(b) Q_R

Fig. 5 Computed Q when AG bolted fault at $t = 0.4$ s

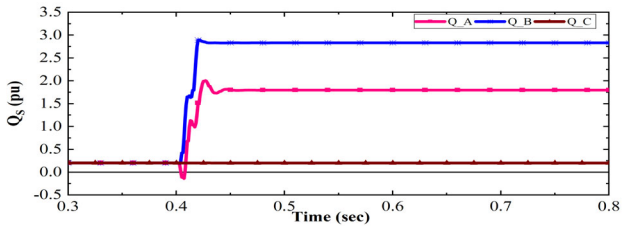

(a) Q_S

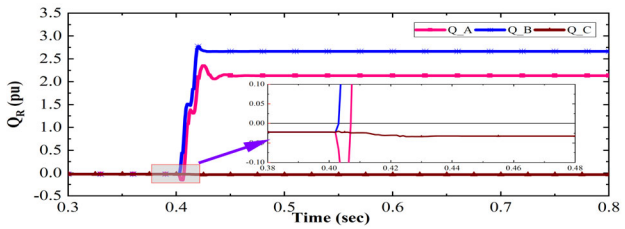

(b) Q_R

Fig. 6 Computed Q when AB-G fault at 0.4 s

In all the fault events, the method has identified the fault within 10 ms after the fault initiation. Hence, the method accurately detects the AG fault with different R_fs. Similarly the proposed method could detect the rest of the PhG faults accurately.

Case (ii): Double Line to Ground Fault (DLG)

ABG fault with a R_f of 10 Ω has been triggered on the TL at 0.4 s with a distance of 0.5 pu from bus S. The obtained waveforms of Q computed at both buses are shown in Fig. 6.

From the graphs shown in Fig. 6a, the Q computed is observed as a positive with a magnitude change in the faulty phases and the Q computed for the individual phase is observed as a positive. Further, the Q of each phase computed from the relay R measurements are exhibited in Fig. 6b.

The sign of Q of all the three phases are negative till the fault inception, and after the fault inception, the sign of Q of both A and B phases are positive and the C phase Q remains

Table 2 Results of A–G fault detection with varied R_fs

S. no.	Fault resistance (Ω)	Sign of Q_S			Sign of Q_R			Fault detection time (ms)
		Q_A	Q_B	Q_C	Q_A	Q_B	Q_C	
1	No fault	+	+	+	–	–	–	NA
2	0.01	+	+	+	+	–	–	7
3	10	+	+	+	+	–	–	9
4	30	+	+	+	+	–	–	9
5	50	+	+	+	+	–	–	10
6	100	+	+	+	+	–	–	10
7	200	+	+	+	+	–	–	10

*NA = not applicable

Table 3 Results of AB-G fault detection with varied R_fs

S. no.	Fault resistance (Ω)	Sign of Q_S			Sign of Q_R			Fault detection time (ms)
		Q_A	Q_B	Q_C	Q_A	Q_B	Q_C	
1	No fault	+	+	+	–	–	–	NA
2	0.01	+	+	+	+	+	–	4
3	10	+	+	+	+	+	–	4
4	30	+	+	+	+	+	–	4
5	50	+	+	+	+	+	–	4
6	100	+	+	+	+	+	–	4
7	200	+	+	+	+	+	–	4

*NA = not applicable

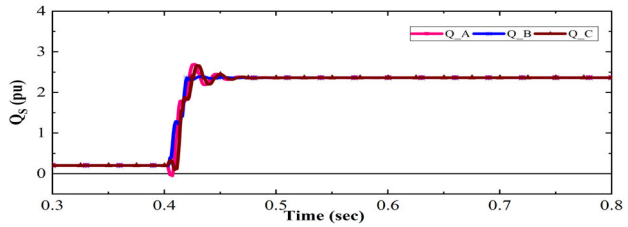

(a) Q_S

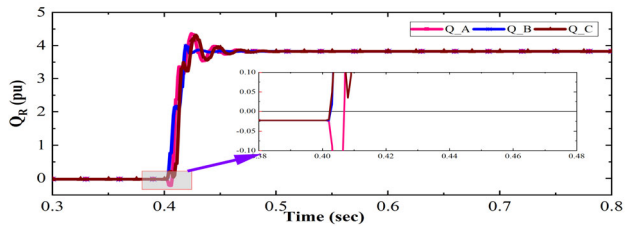

(b) Q_R

Fig. 7 Computed Q when ABC fault at $t = 0.4$ s

negative. Hence, the method detects this situation as a fault on the TL and issues the trip signal. Additionally, the method has been tested with a fault through 0.01 Ω, 10 Ω, 30 Ω, 50 Ω, 100 Ω and 200 Ω resistances and the results obtained are presented in Table 3. From the observations, the method could detect ABG faults within quarter cycle.

Case(iii): Three Phase Fault (LLL)

An ABC fault is initiated at various places on the TL, and the computed Q of each phase has been observed with different faulty situations.

In all the fault cases, the Q of individual three phases at both ends of the lines computed by the suggested approach observed as positive. Figure 7 shows the Q computed by the proposed method when a three-phase fault is created at time equal to 0.4 s on the TL at 0.7 pu distance. After the fault inception, the sign of Q of all the three phases observed from the simulations are found to be positive and the proposed method detects this situation as a fault. Moreover, the proposed method has detected the three-phase fault within 3 ms after fault initiation. Further, the proposed approach has been verified with various R_f from low to high and the corresponding simulation outcomes are presented in Table 4. Hence, it is justified that the proposed approach identifies the ABC faults.

Case (iv): Cross Country Fault (CCF)

CCF is the simultaneous LG faults on any two phases of a TL at two different locations and with same or different FIA [35]. A CCF of two single phase-to-ground faults, AG and BG are initiated at time $t = 0.4$ s at two different locations.

The plots shown in Fig. 8 are the results obtained when a CCF (AG at 0.4 pu and BG at 0.5 pu) triggered on the TL. Figure 8 shows that the Q computed by the proposed method for the faulted phases happened to be simultaneously positive after 0.4 s. Based on the observations, the proposed method issued a trip signal to the circuit breaker. Further, simulations have been done at various locations on the designed TL with dissimilar R_fs to verify the effectiveness of the proposed method for a CCF. Then, the detection time for CCF with fault through various R_fs are presented in Table 5.

Based on the attained outcomes, it is concluded that the method proposed identifies the CCF as well.

4.3 Performance of Fault Detection Methodology with Different FIAs

To check the effectiveness of the proposed method for fault identification, a simulation study has been done with various FIAs.

The graphical representation of three-phase V and Is of both ends of the TL during and after an AG fault inception on the TL at a distance of 0.5 pu with FIA of 45^0 is shown in Fig. 9. From the processed measurements, the Q has been computed, and obtained results are placed in the graph shown

Table 4 Results of ABC fault detection with varied R_f s

S. no.	Fault resistance (Ω)	Sign of Q_S			Sign of Q_R			Fault detection time (ms)
		Q_A	Q_B	Q_C	Q_A	Q_B	Q_C	
1	No fault	+	+	+	–	–	–	NA
2	0.01	+	+	+	+	+	+	3
3	10	+	+	+	+	+	+	3
4	30	+	+	+	+	+	+	3
5	50	+	+	+	+	+	+	3
6	100	+	+	+	+	+	+	3
7	200	+	+	+	+	+	+	3

*NA = not applicable

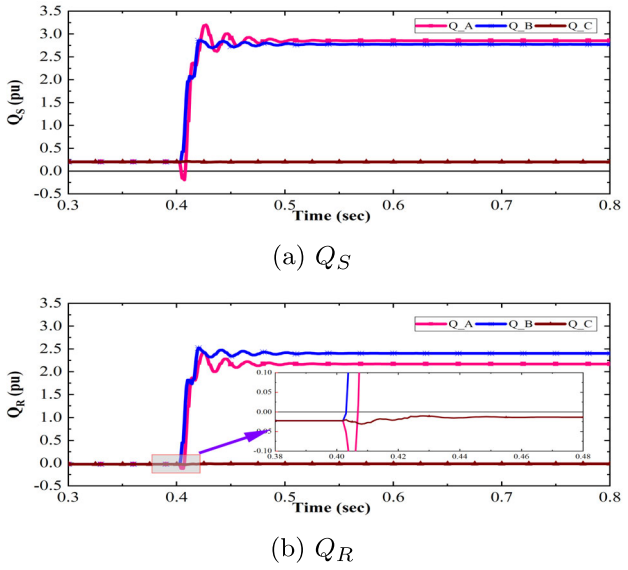

(a) Q_S

(b) Q_R

Fig. 8 Computed Q when CCF at 0.4 s

in Fig. 10. From the results it is clear that the computed Q are positive after the fault inception. Further, the proposed methodology has been verified with various faults with different FIAs and tabulated the simulations outcomes in Table 6. In all these cases, the proposed methodology has correctly

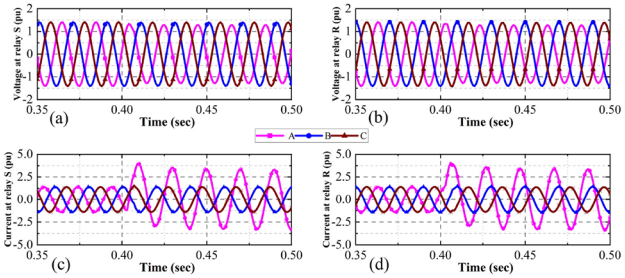

Fig. 9 Measured voltage and currents at bus S and R when AG fault with FIA 45^0

detected the fault. Hence, the suggested method has been examined for the faults with various FIAs.

4.4 Performance of Proposed Method During CT Saturation

The proposed method decision is based on the TL's V and I measurements.

The CT saturation may effect the method's performance. The CTs may get saturated due to the severe fault currents on the TL [36]. Therefore, the suggested method has been tested by initiating various short circuit faults on the TL at different locations with 1000/5A CT with secondary burden 10 Ω, 20

Table 5 Results of CCF detection with varied R_f s

S. no.	Fault resistance (Ω)	Sign of Q_S			Sign of Q_R			Fault detection time (ms)
		Q_A	Q_B	Q_C	Q_A	Q_B	Q_C	
1	No fault	+	+	+	–	–	–	NA
2	0.01	+	+	+	+	+	–	4
3	10	+	+	+	+	+	–	4
4	30	+	+	+	+	+	–	4
5	50	+	+	+	+	+	–	4
6	100	+	+	+	+	+	–	4
7	200	+	+	+	+	+	–	4

*NA = not applicable

Table 6 Faults initiated at different FIAs

S. no.	Fault type	FIA	Sign of Q_S		Sign of Q_R				Fault detection time (ms)
			Q_A	Q_B	Q_C	Q_A	Q_B	Q_C	
1	AG	0^o	+	+	+	+	–	–	7
		45^o	+	+	+	+	–	–	4
		90^o	+	+	+	+	–	–	4
2	ABC	0^o	+	+	+	+	+	+	3
		45^o	+	+	+	+	+	+	3
		90^o	+	+	+	+	+	+	3

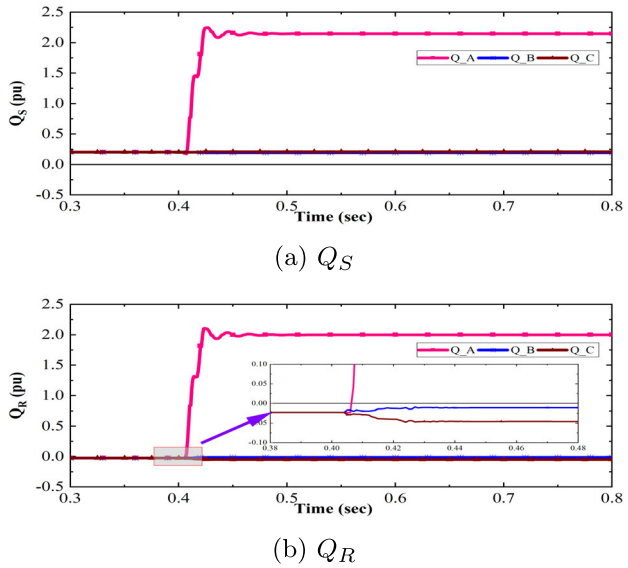

(a) Q_S

(b) Q_R

Fig. 10 Computed Q when AG fault with FIA 45^0

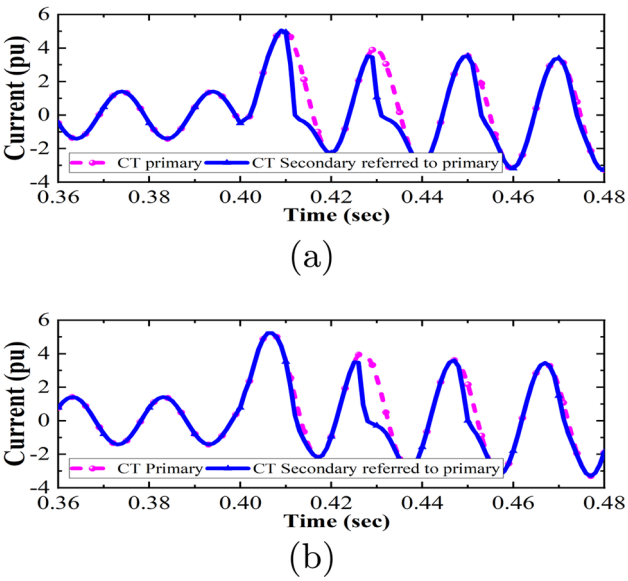

(a)

(b)

Fig. 11 Saturated CT current referred to primary when AG fault at $t = 0.4$ s

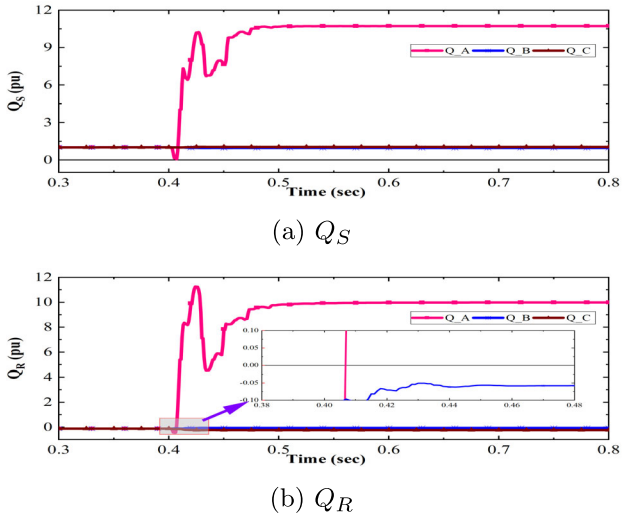

(a) Q_S

(b) Q_R

Fig. 12 Computed Q with CT saturation when AG fault at $t = 0.4$ s

Ω and 30 Ω in the PSCAD/EMTDC and verified the results. It is observed that the current waveforms obtained during CT saturation deviate from unsaturated CT measurements.

Figure 11 shows the phase A secondary currents referred to the primary of CT when phase A to ground fault initiated at 0.4 s with a burden of 30 Ω and the phase A currents with unsaturated CT. The graphical representation of the computed Q shown in Fig. 12 ensures the reliability of the proposed method during CT saturated conditions. Further, various fault cases with CT saturation effect are presented in Table 7.

4.5 Performance of the Proposed Method with Noisy Input

A white Gaussian noise (WGN) of SNR 20, 30 and 40 dBs are considered to check the proposed method's effectiveness during noisy input signal conditions [37].

The considered noise has been added to the measured V and I signals. Further, the noisy signals are used as the inputs and worked through the proposed method, and the obtained results show that the suggested method can identify the fault even during noisy signal situations. To support this claim, the

Table 7 Results with CT saturation condition

S. No.	Fault type	CT burden (Ω)	Sign of Q_S			Sign of Q_R			Fault detection time (ms)
			Q_A	Q_B	Q_C	Q_A	Q_B	Q_C	
1	AG	10	+	+	+	+	–	–	8
		20	+	+	+	+	–	–	8
		30	+	+	+	+	–	–	9
2	ABC	10	+	+	+	+	+	+	3
		20	+	+	+	+	+	+	3
		30	+	+	+	+	+	+	3

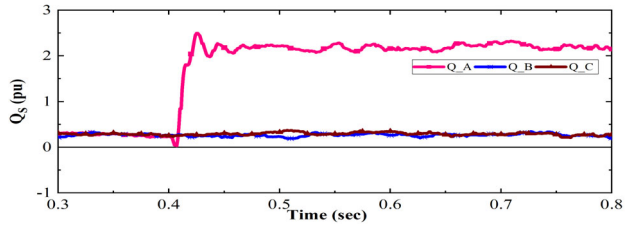

(a) Q_S

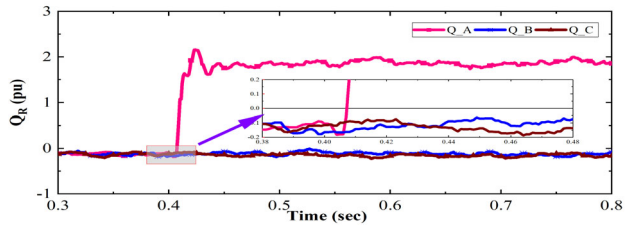

(b) Q_R

Fig. 13 Computed Q with SNR of 20 dB noisy input signals

computed Q at both ends of a line when an AG fault on the TL at 0.4 s with SNR 20 dB noised signal inputs are depicted in Fig. 13. From the simulation outcomes, it is concluded that the noise input signals may not affect the method's decision. Further, the proposed method verified with V and I signals with SNR of 20, 30 and 40 dBs for different fault types. In all situations, the method proposed is found to detect the faults correctly.

4.6 Validation of the Proposed Fault Classification Methodology

After detecting the fault, the proposed method decides the involvement of ground by checking the SIC of either of the relays based on the condition given in the flowchart shown in Fig. 3. After deciding the grounding involvement of a fault, the method classifies the type of fault. To check the performance of the proposed methodology for fault classification, all possible short circuit faults are simulated on a designed TL in PSCAD/EMTDC at various locations on line with different R_fs at different FIAs. In all the fault cases, the proposed method classifies the faults accurately. Further, the simulation results obtained with BG, BC, CAG and ABC faults at a distance of 0.5 pu are shown in Fig. 14 to support the accuracy of the proposed approach.

Figure 14a, b exhibit the computed Q at bus S and bus R before and after the inception of fault. Figure 14a represents the computed Q at bus S of all the three phases and observed as a positive before and after the fault inception at 0.4 s. Further, the Q computed at bus R are shown in Fig. 14b and observed as a negative before the fault inception except B phase. The computed Q of B phase alone is observed as a positive after the fault inception. Therefore, the method classified the fault as BG fault. Figure 14c, d represent the Q computed for all the three phases at bus S before and after fault inception at 0.4 s are positive and the Q computed at bus R until the fault inception are negative, after 0.4 s the B and C phases Q values are observed as a positive. Further, the SIC is happened to be zero. Therefore, the method classifies the fault as a BC fault.

Figure 14e, f shows the computed Q for all the three phases at bus S before and after fault inception at 0.4 s and observed as positive. The Q computed at bus R till the fault inception are negative and after 0.4 s, the C and A phases Q values at bus R are observed as positive. Moreover, the SIC is not equal to zero. Hence, the proposed algorithm classified this as a CAG fault. Figure 14g, h shows the computed Q for all three phases at bus S are observed as a positive irrespective of the fault and normal condition, but the computed three phases Q at bus R till the fault inception are negative, and after 0.4 s the A, B and C phases Q are observed as positive, and the SIC is happened to be equal to zero. Hence, the methodology classifies the fault as ABC. Further, various types of short circuit faults on the TL at distances of 0.1 pu, 0.5 pu and 0.9 pu from bus S with different R_fs are simulated, and the corresponding outcomes are given in Table 8. In all these cases, the proposed method has classified the faults accurately within maximum of one cycle after the fault inception.

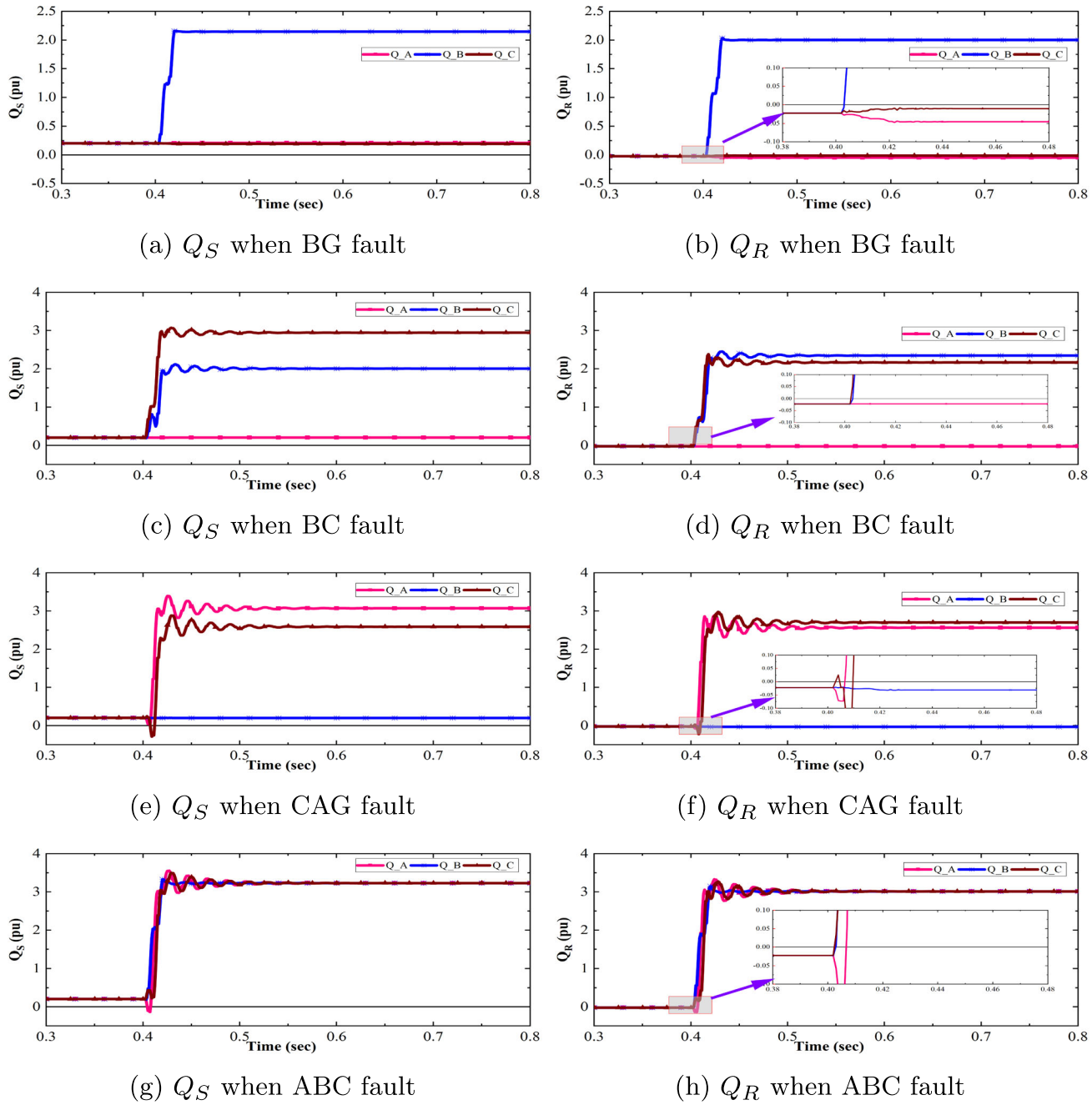

(a) Q_S when BG fault (b) Q_R when BG fault

(c) Q_S when BC fault (d) Q_R when BC fault

(e) Q_S when CAG fault (f) Q_R when CAG fault

(g) Q_S when ABC fault (h) Q_R when ABC fault

Fig. 14 Computed Q of both the relays with different fault scenarios

4.7 Performance of Proposed Methodology with WSCC-9 Bus System

A modified Western System Coordinating Council (WSCC)-9 bus system is considered and designed in PSCAD/EMTDC to confirm the performance of the proposed methodology and the test system used is shown in Fig. 15, the line and source parameters are used from [38] and the f_s of 2 kHz is considered throughout the simulations.

The designed system has been simulated with various types of faults with different R_fs, at different FIAs and at various fault locations on a TL. Apart from these scenarios, the proposed method has also been tested with external faults, CT saturation and noise input signal conditions. In all the scenarios, the proposed method has generated trip signal at appropriate time. To support the efficacy of the proposed approach, the three-phase V and Is, and computed Q at both ends of the line obtained during and after an AG fault initiated at 0.7 s with a distance of 0.5 pu from bus 7 are shown

Table 8 Outcomes of fault classification

S. no.	Fault type, distance, R_f	$(i_A + i_B + i_C) = 0$ (Yes/no)	Sign of Q_S			Sign of Q_R			Fault classified
			Q_A	Q_B	Q_C	Q_A	Q_B	Q_C	
1	AG, 0.5 pu, 500 Ω	No	+	+	+	+	–	–	AG
2	BG, 0.7 pu, 100 Ω	No	+	+	+	–	+	–	BG
3	CG, 0.9 pu, 50 Ω	No	+	+	+	–	–	+	CG
4	ABG, 0.1 pu, 10 Ω	No	+	+	+	+	+	–	ABG
5	BCG, 0.8 pu, 0.01 Ω	No	+	+	+	–	+	+	BCG
6	CAG, 0.5 pu, 500 Ω	No	+	+	+	+	–	+	CAG
7	AB, 0.3 pu, 30 Ω	Yes	+	+	+	+	+	–	AB
8	BC, 0.6 pu, 50 Ω	Yes	+	+	+	–	+	+	BC
9	CA, 0.8 pu, 100 Ω	Yes	+	+	+	+	–	+	CA
10	ABC, 0.9 pu, 200 Ω	Yes	+	+	+	+	+	+	ABC

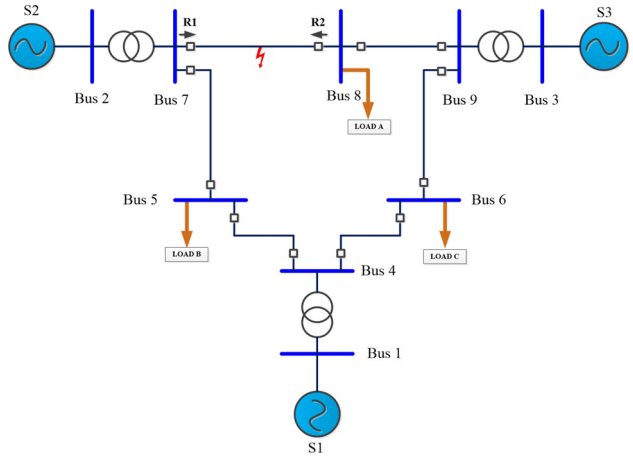

Fig. 15 Modified WSCC-9 bus test system

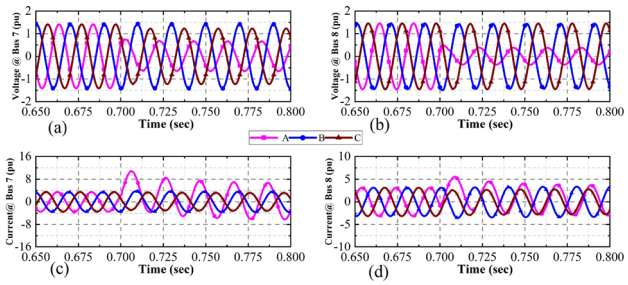

Fig. 16 Three-phase voltages and currents when an AG fault at 0.7 s

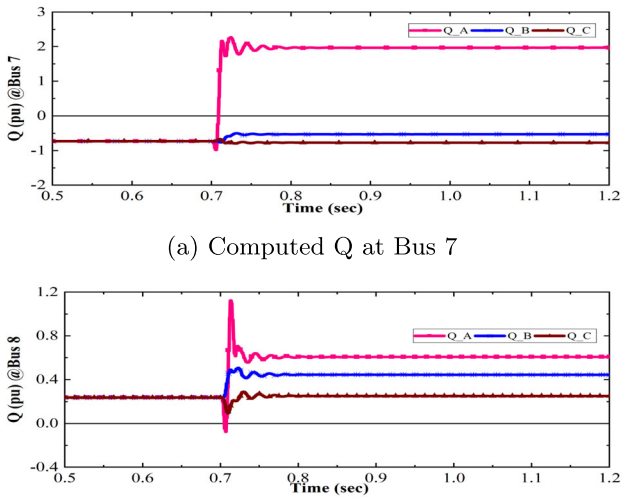

(a) Computed Q at Bus 7

(b) Computed Q at Bus 8

Fig. 17 Computed Q when AG fault at 0.7 s between bus 7 and bus 8

in Figs. 16 and 17, respectively. The plot shown in Fig. 17 shows the computed Q at both the ends of the line when an AG fault on TL. It is observed from the plot that till 0.7 s the computed Q at both ends are positive and negative, respectively. After 0.7 s, the computed sign of Q of phase A is observed as positive at both ends of the line and the proposed method detected this as an AG fault. Further, the results obtained for all short circuit faults with various fault scenarios are recorded in Table 9.

4.8 Performance During External Fault

The proposed method's performance has been verified for an external fault condition by initiating an AG fault at 50 km from bus 8 on the adjacent line (bus 8–bus 9).

The computed Q values are observed before and after the inception of fault, and the same are shown in Fig. 18. The observations show that the Q values computed at both ends of the relays of line 78 (between Bus 7 and Bus 8) are not simultaneously positive. Therefore, the proposed method has not given the trip signal and retains the security of the proposed relay algorithm for external faults.

Table 9 Results of the proposed methodology with modified WSCC-9 bus system

S. no.	Fault type, distance, R_f	$(i_A + i_B + i_C) = 0$ (yes/no)	Sign of Q @ Bus 7			Sign of Q @ Bus 8			Fault detected (yes/no)	Detection time (ms)	Fault classified
			Q_A	Q_B	Q_C	Q_A	Q_B	Q_C			
1	Normal	–	–	–	–	+	+	+	No	NA	No Fault
2	AG, 0.5 pu, 500 Ω	No	+	–	–	+	+	+	Yes	9	AG
3	BG, 0.7 pu, 100 Ω	No	–	+	–	+	+	+	Yes	8	BG
4	CG, 0.9 pu, 50 Ω	No	–	–	+	+	+	+	Yes	7	CG
5	ABG, 0.1 pu, 10 Ω	No	+	+	–	+	+	+	Yes	4	ABG
6	BCG, 0.8 pu, 0.01 Ω	No	–	+	+	+	+	+	Yes	4	BCG
7	CAG, 0.5 pu, 500 Ω	No	+	–	+	+	+	+	Yes	4	CAG
8	AB, 0.3 pu, 30 Ω	Yes	+	+	–	+	+	+	Yes	4	AB
9	BC, 0.6 pu, 50 Ω	Yes	–	+	+	+	+	+	Yes	4	BC
10	CA, 0.8 pu, 100 Ω	Yes	+	–	+	+	+	+	Yes	4	CA
11	ABC, 0.9 pu, 200 Ω	Yes	+	+	+	+	+	+	Yes	3	ABC

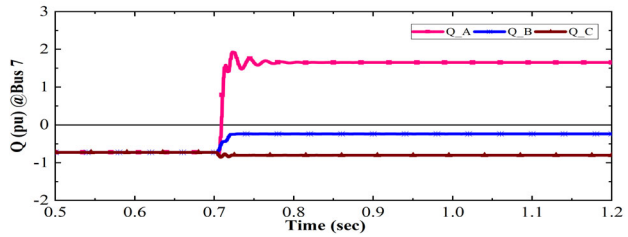

(a) Computed Q at Bus 7

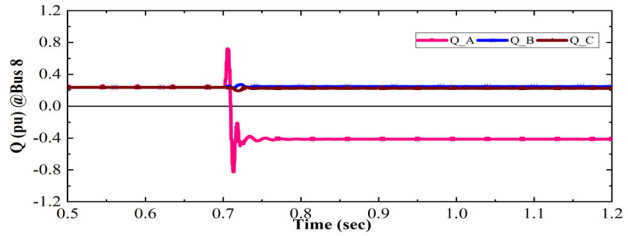

(b) Computed Q at Bus 8

Fig. 18 Computed Q when AG fault on transmission line (Bus 8–Bus 9)

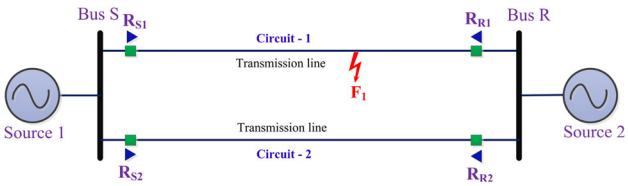

Fig. 19 Double circuit transmission test system

4.9 Validation on Double Circuit Transmission System

A double-circuit line transmission system [39] (Fig. 19) with two sources has been modeled and simulated in the PSCAD / EMTDC software environment. Source and line parameters are considered as per Table 1 and the length of the transmission lines of each circuit is 200 km.

Various faults with different FIAs and at various locations on the transmission line connected between bus-S and bus-R of the circuit-1 have been initiated and the operation of the proposed method has been verified.

To support the validity of the proposed method, an AB fault is initiated on circuit-1 at a location of 0.75 pu from bus-S with zero FIA. In this situation, the sign computed reactive powers at both ends of the circuit-1 have been observed and the graphical representation of the same is shown in Fig. 20. It is evident from Figs. 20 and 21 that the signs of computed reactive powers of all three individual phases of the circuit-1 at both ends till 0.6 s are not simultaneously positive. After the inception of the fault i.e., after 0.6 s, the signs of computed reactive powers of phase A and phase B of circuit-1 are observed as simultaneously positive after 4 ms and the signs

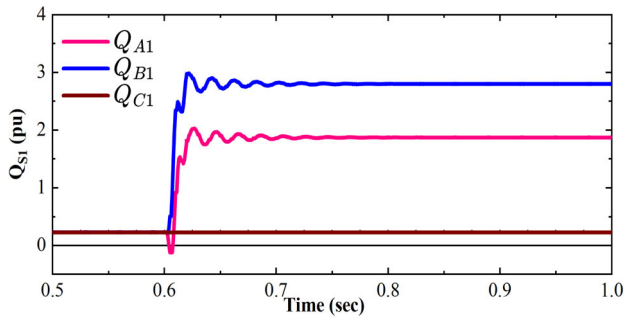

(a) Q_{S1}

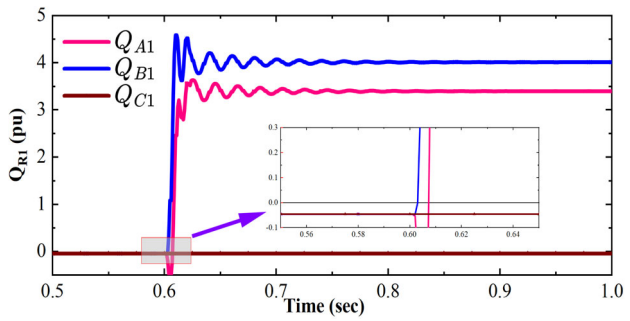

(b) Q_{R1}

Fig. 20 Computed Q during AB fault on transmission line (Circuit-1)

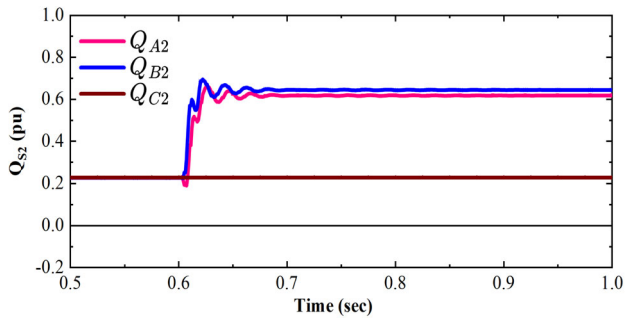

(a) Q_{S2}

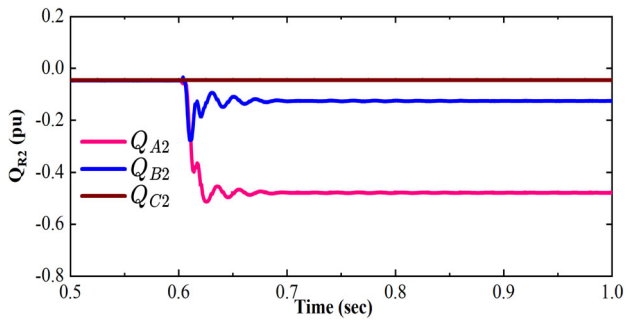

(b) Q_{R2}

Fig. 21 Computed Q during AB fault on transmission line (Circuit-2)

Table 10 Sign of computed Q

Sign	R_{S1}	R_{R1}	R_{S2}	R_{R2}
Q_A	+	+	+	−
Q_B	+	+	+	−
Q_C	+	−	+	−

of computed reactive powers at both the ends of circuit-2 are not simultaneously same. The signs of the computed reactive powers at all the relays are tabulated in Table 10.

Further, the proposed method classified the fault as AB as the sum of instantaneous currents equals zero and computed reactive powers at both ends of phase A and phase B of the circuit-1 are simultaneously positive. In addition, the proposed method has been tested with all other fault cases and abnormal situations. In all test cases, the proposed method retains its essential relaying characteristics such as reliability and sensitivity. It denotes that the proposed method accurately detects and classifies transmission line faults on double-circuit lines.

5 Comparative Study of The Proposed Work with Other Approaches

The proposed method has been compared with the works available in the literature based on the parameters given in Table 11.

[23, 40] are focused on fault detection, and the papers have not addressed about fault classification. The method in [23] is limited to work up to 300 Ω R_f, and the technique depends on line parameters. The method in [40] may mal-operate for sampling frequencies up to 3 kHz during external/reverse faults and also for the single phase-to-ground HIFs at the mid-point of the line. The methods in [41] and [42] are proposed to detect and classify TL faults however both the methods cannot classify the exact faulty phase. The method in [41] is not tested for CT saturation conditions and may mal-operate for external faults, and it is a parameter-dependent algorithm. The method in [42] has not been tested with noisy input signals, CT saturation conditions and external faults. Moreover, the method is limited to work for the faults through R_f up to 100 Ω only. The methods proposed in [43, 44] use the voltages and currents to classify the faults, and the authors of the papers still need to examine the operation of case studies of the proposed method operation during HIF, noise, CT saturation and external faults. In [44], the authors use the sequence components of reactive powers to classify the TL faults. In [45], positive sequence reactive powers at both ends of TL are utilized for fault detection, and the method uses sequence components of currents to classify faults. The authors have yet to investigate the performance of the proposed method

Table 11 Comparative study of the proposed work with the existing approaches

Parameter/reference	[23]	[40]	[41]	[42]	[43]	[44]	[45]	[46]	Proposed scheme
Fault detection	Inv	Inv	Inv	Inv	Inv	N-Inv	Inv	Inv	Inv
Fault classification	N-Inv	N-Inv	Inv*	Inv*	Inv	Inv	Inv	N-Inv	Inv
HIF (Ω)	300	150	300	100	50	100	–	500	500
Change in FIA	Cons	Cons	Cons	Cons	Not Cons	Not Cons	Not Cons	Cons	Cons
Noise	Not Cons	Cons	Cons	Not Cons	Not Cons	Not Cons	Cons	Cons	Cons
CT saturation	Cons	Cons	Not Cons	Not Cons	Not Cons	Not Cons	Not Cons	Cons	Cons
For external faults	Restrain	Mal-Operate	Mal-Operate	N-Inv	N-Inv	N-Inv	N-Inv	Restrain	Restrain
Parameter dependent	Dependent	Independent	Dependent	–	Independent	Independent	Independent	Dependent	Independent
f_s (kHz)	4	10	40	1.92	1	1	–	1.92	1

*Inv = Investigated; N-Inv = Not Investigated; * without faulty phase identification; Cons = Considered

with different FIAs, HIF, CT saturation and external faults. In [46], a differential protection method has been proposed to detect TL faults using reactive power directions, and the fault classification strategy still needs to be addressed. Moreover, the method in [46] is a system dependent one. With the above discussion, it is evident that the methods described are failing with two or more parameters considered in Table 11. The proposed method in this paper gives accurate trip signal and classify the faults even during abnormal situations of the system. Moreover, it is a parameter independent technique. Thus, the proposed approach is found to be superior and outperforms when compared with the existing schemes.

6 Conclusions

An effective fault identification and classification method has been proposed in this article based on the computed reactive powers of both the ends of a TL. The proposed approach estimates the reactive power sign using the fundamental components of the measured V and I signals. For fault detection, the method gives trip signal if the computed sign of reactive powers at both ends are positive. The method classifies the fault based on the strategy developed in this paper. Further, the proposed method is validated on a two-bus transmission test system, double-circuit transmission system and a modified WSCC-9 bus transmission test system using PSCAD/EMTDC and MATLAB/Simulink softwares. The proposed method has detected all types of TL faults, including CCFs and it effectively working at different scenarios such as high impedance faults, different FIAs, noisy inputs signal, CT saturation, and sudden change in load and accurately detecting the faults within a half cycle. Further, The method classifies all shunt faults within one cycle for all the above-mentioned abnormal conditions. The results denote that the proposed method is reliable compared with other methods mentioned in the literature.

Author Contributions Rajesh Velpula: Investigation, Conceptualization, Methodology, Software, Data curation, Writing—Original draft; N Nageswara Reddy: Investigation, Conceptualization, Methodology, Software, Data curation, Writing—Original draft.; Raja Pitchaimuthu: Supervision, formal analysis, Validation, Writing—Review and Editing.

Funding Not applicable.

Data availibility Data will be made available on request.

Declarations

Conflict of interest The authors declare that they have no known competing financial interests or personal relationships that could have appeared to influence the work reported in this paper.

Ethical approval Not applicable.

Consent for publication The authors have read and understood the publishing policy and submitted the manuscript in accordance with this policy.

References

1. Biswas, S.; Nayak, P.K.: A fault detection and classification scheme for unified power flow controller compensated transmission lines connecting wind farms. IEEE Syst. J. **15**(1), 297–306 (2021). https://doi.org/10.1109/JSYST.2020.2964421
2. Li, Z.; Tong, N.; Lin, X.; Wang, Z.; Zheng, Y.; Lyu, R.; Zhao, H.; Chen, L.: Enhanced summation impedance relay for EHV transmission lines. IEEE Trans. Power Delivery **34**(3), 807–818 (2019). https://doi.org/10.1109/TPWRD.2019.2902388
3. Namdari, F.; Salehi, M.: High-speed protection scheme based on initial current traveling wave for transmission lines employing mathematical morphology. IEEE Trans. Power Delivery **32**(1), 246–253 (2017). https://doi.org/10.1109/TPWRD.2016.2571341
4. Chen, M.; Wang, H.; Shen, S.; He, B.: Research on a distance relay-based wide-area backup protection algorithm for transmission lines. IEEE Trans. Power Delivery **32**(1), 97–105 (2017). https://doi.org/10.1109/TPWRD.2016.2599198
5. Prasad, A.; Belwin Edward, J.; Ravi, K.: A review on fault classification methodologies in power transmission systems: Part—i. J. Electr. Syst. Inf. Technol. **5**(1), 48–60 (2018). https://doi.org/10.1016/j.jesit.2017.01.004
6. Prasad, A.; Belwin Edward, J.; Ravi, K.: A review on fault classification methodologies in power transmission systems: Part-II. J. Electr. Syst. Inf. Technol. **5**(1), 61–67 (2018). https://doi.org/10.1016/j.jesit.2016.10.003
7. Babu, K.; Tripathy, M.; Singh, A.: Recent techniques used in transmission line protection: a review. Int. J. Eng. Sci. Technol. **3**(3), 1–8 (2011). https://doi.org/10.4314/ijest.v3i3.68416
8. Mishra, D.P.; Ray, P.: Fault Detection, Location and Classification of a Transmission Line, vol. 30, pp. 1377–1424. Springer, Berlin (2018). https://doi.org/10.1007/s00521-017-3295-y
9. Megahed, A.I.; Moussa, A.M.; Bayoumy, A.E.: Usage of wavelet transform in the protection of series-compensated transmission lines. IEEE Trans. Power Delivery **21**(3), 1213–1221 (2006). https://doi.org/10.1109/TPWRD.2006.876981
10. Valsan, S.P.; Swarup, K.S.: Wavelet transform based digital protection for transmission lines. Int. J. Electr. Power Energy Syst. **31**(7–8), 379–388 (2009). https://doi.org/10.1016/j.ijepes.2009.03.024
11. Shu, H.; Tian, K.; Tang, Y.; Dai, Y.: Novel protection scheme for EHV transmission line based on traveling wave energy. Electr. Power Syst. Res. **230**, 110247 (2024). https://doi.org/10.1016/j.epsr.2024.110247
12. Hudomalj, M.; Trost, A.; Čampa, A.: Traveling wave method for event localization and characterization of power transmission lines. Electr. Power Syst. Res. **232**, 110382 (2024). https://doi.org/10.1016/j.epsr.2024.110382
13. Fahim, S.R.; Sarker, Y.; Sarker, S.K.; Sheikh, M.R.I.; Das, S.K.: Self attention convolutional neural network with time series imaging based feature extraction for transmission line fault detection and classification. Electr. Power Syst. Res. **187**(May), 106437 (2020). https://doi.org/10.1016/j.epsr.2020.106437
14. Tong, H.; Qiu, R.C.; Zhang, D.; Yang, H.; Ding, Q.; Shi, X.: Detection and classification of transmission line transient faults based on graph convolutional neural network. CSEE J. Power Energy Syst. **7**(3), 456–471 (2021). https://doi.org/10.17775/CSEEJPES.2020.04970
15. Vyas, B.Y.; Maheshwari, R.P.; Das, B.: Versatile relaying algorithm for detection and classification of fault on transmission line. Electric Power Syst. Res. **192**, 106913 (2021). https://doi.org/10.1016/j.epsr.2020.106913
16. Fahim, S.R.; Sarker, S.K.; Muyeen, S.M.; Das, S.K.; Kamwa, I.: A deep learning based intelligent approach in detection and classification of transmission line faults. Int. J. Electr. Power Energy Syst. **133**, 107102 (2021). https://doi.org/10.1016/j.ijepes.2021.107102
17. Mukherjee, A.; Kundu, P.K.; Das, A.: Classification and localization of transmission line faults using curve fitting technique with Principal component analysis features. Electr. Eng. **103**(6), 2929–2944 (2021). https://doi.org/10.1007/s00202-021-01285-7
18. Chen, K.; Hu, J.; He, J.: Detection and Classification of Transmission Line Faults Based on Unsupervised Feature Learning and Convolutional Sparse Autoencoder. IEEE Trans. Smart Grid **9**(3), 1748–1758 (2018). https://doi.org/10.1109/TSG.2016.2598881
19. Najafzadeh, M.; Pouladi, J.; Daghigh, A.; Beiza, J.; Abedinzade, T.: Fault detection, classification and localization along the power grid line using optimized machine learning algorithms. Int. J. Comput. Intell. Syst. (2024). https://doi.org/10.1007/s44196-024-00434-7
20. Bhatnagar, M.; Yadav, A.; Swetapadma, A.; Abdelaziz, A.Y.: LSTM-based low-impedance fault and high-impedance fault detection and classification. Electr. Eng. (2024). https://doi.org/10.1007/s00202-024-02381-0
21. Biswal, S.; Biswal, M.; Malik, O.P.: Hilbert Huang transform based online differential relay algorithm for a shunt-compensated transmission line. IEEE Trans. Power Delivery **33**(6), 2803–2811 (2018). https://doi.org/10.1109/TPWRD.2018.2827843
22. Gupta, A.; Pachar, R.K.; Khan, B.; Mahela, O.P.; Padmanaban, S.: A multivariable transmission line protection scheme using signal processing techniques. IET Gener. Transm. Distrib. **15**(22), 3115–3137 (2021). https://doi.org/10.1049/gtd2.12244
23. Chatterjee, B.; Debnath, S.: A new protection scheme for transmission lines utilizing positive sequence fault components. Electric Power Syst. Res. **190**, 106847 (2021). https://doi.org/10.1016/j.epsr.2020.106847
24. Mirhosseini, S.S.; Akhbari, M.: Wide area backup protection algorithm for transmission lines based on fault component complex power. Int. J. Electr. Power Energy Syst. **83**, 1–6 (2016). https://doi.org/10.1016/j.ijepes.2016.03.056
25. Velpula, R.; Reddy, N.N.; Hareesh, S.V.; Pitchaimuthu, R.: A simple approach for the protection of EHV transmission lines. Electric Power Syst. Res. **224**(July), 109744 (2023). https://doi.org/10.1016/j.epsr.2023.109744
26. Gangolu, S.; Sarangi, S.: A new differential current protection algorithm for three-terminal line. Arab. J. Sci. Eng. **47**(11), 14075–14085 (2022). https://doi.org/10.1007/s13369-022-06630-x
27. Kumar, B.R.; Mohapatra, A.; Chakrabarti, S.; Kumar, A.: Phase angle-based fault detection and classification for protection of transmission lines. Int. J. Electr. Power Energy Syst. **133**(May), 107258 (2021). https://doi.org/10.1016/j.ijepes.2021.107258
28. Chavez, J.J.; Kumar, N.V.; Azizi, S.; Guardado, J.L.; Rueda, J.; Palensky, P.; Terzija, V.; Popov, M.: PMU-voltage drop based fault locator for transmission backup protection. Electric Power Syst. Res. **196**, 107188 (2021). https://doi.org/10.1016/j.epsr.2021.107188
29. Sharma, J.P.; Gupta, O.H.; Tripathy, M.: A new sequence current-based adaptive pilot relaying scheme for modern HVAC transmission lines. Electr. Power Compon. Syst. **49**(1–2), 32–47 (2021). https://doi.org/10.1080/15325008.2021.1937394
30. Gangolu, S.; Sarangi, S.; Mohanty, R.: Relay algorithm for STATCOM compensated line using differential current ratio. Int. J. Electr. Power Energy Syst. **155**(PA), 109473 (2024). https://doi.org/10.1016/j.ijepes.2023.109473
31. Deng, H.; Lin, R.; Cui, J.: Identification of symmetrical faults and overloads on parallel transmission lines based on compensated volt-

age cosine volume. Electr. Eng. (2024). https://doi.org/10.1007/s00202-024-02289-9
32. Kundur, P.; Balu, N.J.; Lauby, M.G.: Power System Stability and Control. EPRI Power System Engineering Series. McGraw-Hill Education, New York (1994)
33. Jena, M.K.; Samantaray, S.R.; Panigrahi, B.K.: A new wide-area backup protection scheme for series-compensated transmission system. IEEE Syst. J. **11**(3), 1877–1887 (2017). https://doi.org/10.1109/JSYST.2015.2467218
34. Caballero, P.T.; Costa, E.C.M.; Kurokawa, S.: Frequency-dependent multiconductor line model based on the Bergeron method. Electric Power Syst. Res. **127**, 314–322 (2015). https://doi.org/10.1016/j.epsr.2015.05.019
35. Saber, A.; Emam, A.; Elghazaly, H.: Wide-area backup protection scheme for transmission lines considering cross-country and evolving faults. IEEE Syst. J. **13**(1), 813–822 (2019). https://doi.org/10.1109/JSYST.2018.2827938
36. Zhang, G.; Tong, X.; Hong, Q.; Booth, C.D.: Waveform similarity-based robust pilot protection for transmission lines. IEEE Trans. Power Delivery **37**(3), 1856–1865 (2022). https://doi.org/10.1109/TPWRD.2021.3099348
37. Gil, M.; Abdoos, A.A.; Sanaye-Pasand, M.: A precise analytical method for fault location in double-circuit transmission lines. Int. J. Electr. Power Energy Syst. **126**(1), 106568 (2021). https://doi.org/10.1016/j.ijepes.2020.106568
38. Nayak, P.K.; Pradhan, A.K.; Bajpai, P.: A fault detection technique for the series-compensated line during power swing. IEEE Trans. Power Delivery **28**(2), 714–722 (2013). https://doi.org/10.1109/TPWRD.2012.2231886
39. Mahamedi, B.; Zhu, J.G.: Unsynchronized fault location based on the negative-sequence voltage magnitude for double-circuit transmission lines. IEEE Trans. Power Delivery **29**(4), 1901–1908 (2014). https://doi.org/10.1109/TPWRD.2013.2294972
40. Jarrahi, M.A.; Samet, H.; Ghanbari, T.: Fast current-only based fault detection method in transmission line. IEEE Syst. J. **13**(2), 1725–1736 (2019). https://doi.org/10.1109/JSYST.2018.2822549
41. Wijekoon, J.; Rajapakse, A.D.; Haleem, N.M.: Fast and reliable method for identifying fault type and faulted phases using band limited transient currents. IEEE Trans. Power Delivery **36**(5), 2839–2850 (2021). https://doi.org/10.1109/TPWRD.2020.3027793
42. Rathore, B.; Mahela, O.P.; Khan, B.; Alhelou, H.H.; Siano, P.: Wavelet-alienation-neural-based protection scheme for STATCOM compensated transmission line. IEEE Trans. Industr. Inf. **17**(4), 2557–2565 (2021). https://doi.org/10.1109/TII.2020.3001063
43. Mahamedi, B.: A novel setting-free method for fault classification and faulty phase selection by using a pilot scheme. In: 2011 2nd International Conference on Electric Power and Energy Conversion Systems, EPECS 2011, pp. 1–6 (2011) https://doi.org/10.1109/EPECS.2011.6126835
44. Khadke, P.; Patne, N.; Bolisetty, S.: Fault Classification and Faulty Phase Selection Using Symmetrical Components of Reactive Power for EHV Transmission Line, vol. 698, pp. 31–42. Springer, Singapore (2019). https://doi.org/10.1007/978-981-13-1819-1_4
45. Rahmati, A.; Adhami, R.: A fault detection and classification technique based on sequential components. IEEE Trans. Ind. Appl. **50**(6), 4202–4209 (2014). https://doi.org/10.1109/TIA.2014.2313652
46. Dantas, D.T.; Pellini, E.L.; Manassero, G.: Time-domain differential protection method applied to transmission lines. IEEE Trans. Power Delivery **33**(6), 2634–2642 (2018). https://doi.org/10.1109/TPWRD.2018.2841342